



Investigation and prediction of central cracking in cross wedge rolling

Xiyan Zhou^{1,2} · Chaoyang Sun³ · Baoyu Wang³ · Jun Jiang¹

Received: 31 May 2022 / Accepted: 8 September 2022 / Published online: 26 September 2022
© Crown 2022

Abstract

Central cracking refers to the formation of internal cavities in cross wedge rolling (CWR) products. It occurs in various materials such as aluminium/titanium alloys, steels and plasticine at room or elevated temperatures, driven by different central cracking mechanisms. However, these mechanisms are still elusive, and a unified central cracking predictive model is absent due to the complex stress states within the workpiece, including triaxial stress states, cyclic loading and severe shear effects. In this study, the underlying fracture mechanisms were revealed, and a robust unified damage model with sound physical meanings was developed using a lab-scale CWR physical model and finite element models. The physical model with the plasticine billets was built, allowing the CWR dies with different geometries rapidly 3D printed and the billets with various ductility efficiently manufactured. The central cracking transiting from brittle to ductile fracture was experimentally observed for the first time using specifically designed plasticine/flour composite samples at varying ductility. The corresponding physics-based central cracking predictive model was proposed and validated quantitatively with 60 groups of CWR tests and compared with ten existing damage models/fracture criteria. This study effectively solves the long-lasting central cracking problem in the CWR industry and enhances the scientific understanding of fracture mechanics in complex engineering applications.

Keywords Cross wedge rolling · Central cracking · Fracture mechanism · Fracture criterion · Physical model

1 Introduction

Cross wedge rolling (CWR), an innovative metal forming process for manufacturing axial symmetrical stepped shafts/axles, is gaining high popularity in industries such as the automotive, high-speed railway, and aerospace. CWR is advantageous in many aspects such as high productivity, high material utilisation and low energy consumption, compared to the conventional forging processes such as press forging or machining [1, 2]. The material utilisation of CWR can reach 0.8–0.98 [3]. New CWR-related technologies are being developed quickly. For example, Ji et al. [4] experimentally verified the capability of producing

hollow parts by using CWR with mandrels. Zheng et al. [5] and Pater et al. [6] produced shafts with non-circular cross-section or normal/skew teeth using CWR, respectively. Bulzak et al. [7] compared the ball pins manufactured in hot and warm temperature. CWR products with corrugated surface were produced [8]. The composite CWR shafts made by 42CrMo and Q235 was studied in terms of deformation characteristics and effects of process parameters [9, 10]. The new technologies drive the market demand in CWR expanding sharply.

Central cracking, the formation of cavities in the central region of CWR products along the axial direction, is a critical problem impeding its further development in safety-critical industries such as the aerospace industry. Central cracking has been observed and investigated in a wide range of materials, e.g. steels, aluminium, titanium and plasticine. For example, Li et al. [11] and Li and Lovell [12] discovered the central crack morphologies in pure aluminium and considered the tensile and shear stresses contributed to the central crack formation. Yang et al. [13] investigated the central crack evolution in C45 steels on a microscopic scale and attributed the central crack formation to the tensile

✉ Jun Jiang
jun.jiang@imperial.ac.uk

¹ Department of Mechanical Engineering, Imperial College London, Exhibition Road, London SW7 2AZ, UK

² Department of Mechanical and Industrial Engineering, NTNU, 7491 Trondheim, Norway

³ School of Mechanical Engineering, University of Science and Technology Beijing, Beijing 100083, China

and shear stresses. The effects of shear stress cycle and the first principal stress were emphasised in generating internal voids by experiments and simulations in multi-wedge CWR by Zhou et al. [14]. Pater et al. [15, 16] revealed that the central crack mechanism in C45 steels involved void formation and shear fracture by numerically analysing the stress triaxiality (the ratio of mean stress over the von Mises stress) range. Zhou et al. [17] confirmed the dominant role of the maximum shear stress in central crack formation by investigating the stress states on the plasticine workpiece under different central crack conditions. It is well known that the fracture mechanisms vary with the material property, such as ductility. For instance, the fracture mode of steel transitions from brittle to ductile with the increase of temperature due to improved ductility [18]. However, little research has been conducted to reveal the underlying multiple central crack mechanisms. Thus, it is necessary to identify the multiple central crack mechanisms in order to build a robust unified physic-based damage model.

Central cracking micromechanics has been researched recently. Experimentally, Yang et al. [13] observed the voids nucleated around the inclusions, grew, coalesced and led to final fracture. Zhou et al. [19] quantitatively validated the critical effect of inclusions on central cracking. Pater et al. [16] clarified the co-existing fracture mechanisms, void formation and shear fracture, by analysing the stress triaxiality. However, these micromechanics understandings have not been involved in existing central cracking predictive models. Thus, it is necessary to introduce micromechanics into the central crack model to achieve high prediction accuracy based on sufficient physical meanings.

The prediction models have brought great conveniences to the industries by reducing the time and costs on error and trials. For example, the rolling force can be predicted easily and accurately with the prediction models newly developed by Zhang et al. [20, 21]. Similarly, many damage models and fracture criteria have been introduced and applied to predict the central cracks for manufacturing crack-free products. Li and Lovell [22] suggested that the equivalent plastic strain was an accurate criterion by comparing the stress/strain states in pure aluminium samples produced by using two die geometries. The phenomenological damage models for ductile fracture, such as Cockcroft and Latham (C&L) model, normalised C&L model and Oyane model, are extensively applied in predicting central cracking with high accuracy to some degrees. A density change model was applied to clarify the forming windows to prevent central cracks [23]. Recently, Pater et al. [16] proposed a damage model considering the fracture mechanisms, void formation and shear fracture, achieving high accuracy in C45 steel at the elevated temperature. Zhou et al. [24] proposed a physics-based fracture criterion capable of predicting the central cracks in 27 groups of CWR tests on pure aluminium AA1100 with

different die geometries. However, these models have never been validated by different materials, which exhibit different fracture mechanisms.

Meanwhile, great progress has been witnessed in developing physics-based damage models for predicting shear dominant ductile fracture. Smith et al. [25] expanded the application of the Rice and Tracey model into the low or negative triaxiality stress states by involving the void shrinking mechanism. Zhu and Engelhardt [26] introduced a new term of shear ratio into the R&T model to describe the damage caused by shear effects. Bao and Wierzbicki [27] found that the fracture locus varies with triaxiality significantly based on experiments under various stress states. Xue and Wierzbicki [28] (X&W) modified the plastic strain criterion by considering triaxiality and Lode parameters, covering the whole range of stress states and accounting for the material ductility. Bai and Wierzbicki [29] converted the conventional Mohr–Coulomb criterion to the space of the triaxiality, Lode angle parameter and equivalent von Mises stress, enabling to predict fracture nucleation in a much wider range of stress states. However, little progress has been seen on the fracture under non-proportional loadings on the onset of ductile fracture. Bai [30] found the importance of non-linear loading paths on ductile fracture onset and modified the accumulation law of damage considering non-proportional loading histories. Benzerga et al. [31] also demonstrated the significance of the loading path on the fracture strain by conducting unit cell computations. Faleskog and Barsoum [32] noticed a decrease in ductility during the stress triaxiality interval [0, 0.33] by conducting tension–torsion experiments. Papisidero et al. [33] conducted tension–torsion experiments on tubular specimens and validated that a Hosford–Coulomb-based non-linear damage law can describe the effect of non-proportional loadings on fracture strain. The above models show advances in predicting shear-dominated ductile fracture under non-proportional loadings. Therefore, it is worth testing their robustness in predicting central cracking in CWR.

Model materials such as plasticine are widely used in physically simulating metal forming processes. Chijiwa et al. [34] and Wong et al. [35] experimentally revealed their similarities to metals in terms of constitutive behaviours, frictional behaviours and fracture features. The softness of the model materials enables laboratory-scale reproduction to be achieved, whereby the tools can be rapidly 3D printed. Wójcik et al. [36] built the physical CWR model with 3D printed dies. Zhou et al. [37, 38] approved the feasibility of differential velocity sideways extrusion using plasticine and conducted the geometrical parametrical study. Physical models have been applied to study the CWR since 1984, when the internal defects were simulated in a rotary side-compression test with plasticine by Danno and Tanaka [39]. Fu and Dean [40] investigated the necking and twisting by using plasticine. Recently, Pater et al. [41] and Wójcik et al. [36] achieved high similarities between the commercial plasticine and

hot steels (1150 °C) in terms of mechanical properties and defect features in CWR. Besides the temperature, the composition in plasticine is also adjustable for achieving desired mechanical properties of the modelled materials. Hawryluk et al. [42] compared the mechanical properties of plasticine with different compositions. Zhou et al. [17] designed the novel plasticine/flour composites to build the CWR billets and investigated the underlying central crack mechanism under various stress states. Thus, using model materials is reasonable to investigate the multiple fracture mechanisms and criteria in CWR.

This work aims to reveal the multiple central crack mechanisms, build a unified physics-based fracture criterion and examine their accuracy in different materials. The multiple fracture mechanisms will be investigated using newly designed plasticine/flour composites with a lab-scale CWR machine. The fracture criterion for both the high and low ductility material will be proposed considering the multiple fracture mechanisms such as the central crack in pure aluminium at room temperature and in the hot steels at elevated temperature. Its robustness will be compared with ten existing damage models and validated by CWR tests in various materials.

2 Proposal of a new central crack criterion

A physics-based central crack criterion is proposed as presented in Eqs. (1) and (2). It can be used to predict the central crack in both low and high ductility materials. Brittle materials are excluded in this study as they are rarely used in the CWR process in practice. Different central cracking mechanisms involve in different materials at cold, warm or hot CWR processes. It is defined that central cracking occurs when the stress intensity in low ductility materials or the accumulated damage value in high ductility materials reaches the critical value. The stress intensity factor and the damage value are represented by the item D , with the critical value being D_c . After normalisation, the criterion can be written as Eq. (1), where the normalised value is represented by D_n . When the material is at low ductility, the stress-based fracture criterion will be applied as presented in Eq. (2). In this equation, A and B are material constants, presenting the contribution ratios of the maximum shear stress τ_m and the first principal stress σ_1 to central crack formation. Zhou et al. [17, 24] has validated this criterion by using low ductility materials, including 27 groups of pure aluminium (highly strained) CWR tests and 16 groups of CWR tests with plasticine/flour composites. When the material is at high ductility, an energy-based fracture criterion will be employed considering the severe plastic deformation occurs before final fracture, as presented in Eq. (2). The energy-based damage value D consists of two parts representing

two fracture mechanisms, shear fracture and void formation. Here, σ_m represents the mean stress and $\bar{\varepsilon}_p$ is the equivalent plastic strain. Zhou et al. [24] experimentally validated the significant effect of the maximum shear stress τ_m in central cracking. The significance of the mean stress σ_m in presenting void growth has been well understood such as in the R&T model. A linear relationship between shear fracture and void formation with a coefficient C is applied to describe their interactive effects on accumulated damage due to its computational and experimental calibration efficiency. Both the critical damage value D_c and the coefficient C depend on material properties, which can be calibrated by CWR tests with simplified CWR dies. The simplified CWR test can well simulate the commercial CWR process by simulating the stress states including cyclic loading, severe plastic deformation and triaxial stress states. More details about the proposal and feasibility of this novel method can be found in Zhou et al. [24]. The calibration of the material constants includes three steps: (i) conducting interrupted CWR tests with dies under two feed angles and determining the locations for the void nucleation; (ii) simulating the corresponding processes via FEM and determining both the first principal stress and maximum shear stress at the void nucleation location under two feed angles; and (iii) inputting the two groups of data into the proposed fracture criterion and calculating the material constants. For each specific material, the calibration test should be taken once, as the material constant is material dependent, which can be sensitive to the temperature. For the strain rate-dependent materials, the stress strain data under different strain rates should be obtained and applied to describe the material model in FEM. The strain rate sensitivity and flour weight ratios resulted hardening effects in this study are implicitly embedded in the stress–strain behaviours of materials, which are fully accounted in our FE simulation. The FE simulation-determined shear and normal stress components are used in the proposed criterion.

The low and high ductility materials in this study are distinguished based on different central cracking mechanisms, which is systematically presented in Sect. 5.1. In practice, it can be easily distinguished by the morphologies of the central cracks. If they are surrounded by numerous appreciable voids, the materials are considered as high ductility materials, such as C45 steel at elevated temperature (1150 °C). If more cleavage and smoother tips are involved, the materials can be defined as low ductility materials, such as highly strained pure aluminium (AA1100H16) at room temperature.

$$D_n = D/D_c \geq 1 \quad (1)$$

$$D = \begin{cases} A\tau_m + B\sigma_1; (A + B = 1) & \text{Low ductility materials} \\ \int_0^{\bar{\varepsilon}_f} (\tau_m + C\sigma_m) d\bar{\varepsilon}_p; & \text{High ductility materials} \end{cases} \quad (2)$$

3 Methodology

A laboratory-scale CWR physical model was built to reproduce the industrial CWR process. The plasticine and flour composites were designed and applied to investigate the central cracking behaviours with various ductility and die geometries. The corresponding CWR FE models were established to investigate the stress/strain and damage distribution and evolution. The robustness of the proposed fracture criterion was validated by comparing the predicted damage with the experimental central cracking behaviours by using the plasticine flour composite samples and the C45 steels at high temperature. Besides, ten existing fracture criteria were also examined and compared. To validate the robustness of the proposed fracture criterion, 60 groups of CWR tests were considered.

3.1 Physical model

3.1.1 Materials

Plasticine samples with various flour contents were employed for the investigation of the multiple fracture mechanisms. Plasticine from Flair Company was selected due to its stable feature (never dries out). The plasticine from the same batch was selected to keep the high consistency in chemical compositions and mechanical properties.

Uniaxial tensile tests were conducted using Instron 5543 to obtain the mechanical properties of the newly designed plasticine materials. The setup is shown in Fig. 1a. A 1000-g load cell was used to ensure the measurement accuracy. The speed range of this machine is 0.05–1000 mm/s with the crosshead speed accuracy $\pm 0.1\%$. The load and strain measurement accuracy can reach $\pm 0.5\%$. New grips with inner steps were designed to ensure the plasticine specimen was firmly clamped without slippage during the test, as presented in Fig. 1b. The grips were 3D printed with a plastic polymer material, polylactic acid (PLA), using a 3D printer Fortus 400mc. The structure of the tensile test plasticine specimen is presented in Fig. 1c.

Each test was repeated at least three times to ensure the test reproducibility. Figure 2a shows the engineering stress–strain curves of the plasticine with varying flour weight ratios. The stress–strain data were converted from the load and displacement recorded on the tensile test machine, which can show the general trend between the different flour weight ratios that the increase of the flour contents generally reduces the ductility of the samples. The strain rate here was set to be 0.5/s (estimated value calculated by tensile speed/gauge length), corresponding to the average strain rate of the CWR sample during the test. Figure 2b presents the true stress–strain curves of pure plasticine (without any flour)

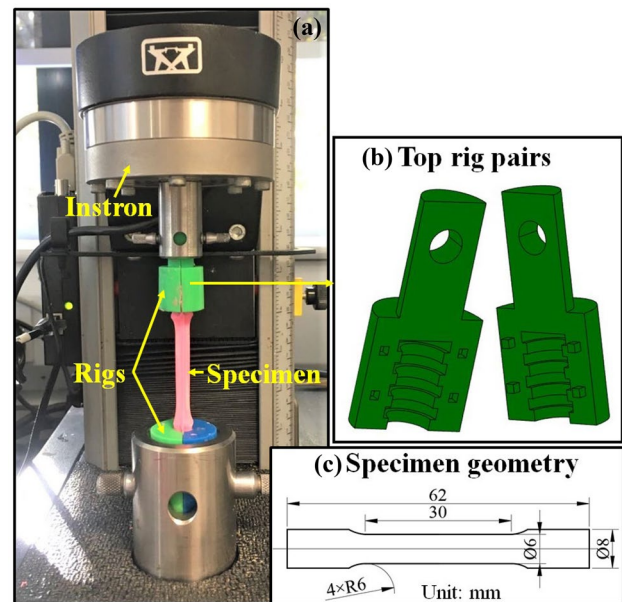


Fig. 1 Uniaxial tensile tests for plasticine: **a** setup and structures of **b** 3D printed grips and **c** specimen. (in colour)

at different strain rates, showing the material yield/ultimate strengths rise with the increase of the strain rate, which is consistent with the material behaviours of hot steels.

3.1.2 Cross wedge rolling prototype

The lab-scale CWR prototype is presented in Fig. 3. A cylindrical billet is placed in the middle of two flat dies. The upper die is fixed on the frame, while the bottom die is driven forward by the electronically controlled step motor at a speed of 20 mm/s. Driven by the strong tangential force from the dies, the billet is self-rotated and moved forward at a speed of approximately 10 mm/s during the test. After the rolling, the initial cylindrical billet is deformed into a stepped shaft. The initial dimension of the billet is $\Phi 25.4 \text{ mm} \times 50 \text{ mm}$. The plasticine billets were carefully prepared. Firstly, the plasticine and flour were thoroughly mixed for a certain time using a food mixer. Then, the plasticine and flour composites were subjected with over 10 cycles of folding, rolling and hammering for homogenising the structure, followed by press forging with a pair of 3D printed dies to guarantee the geometry accuracy.

The dies with various geometries were rapidly manufactured by a 3D printer using the acrylonitrile butadiene styrene (ABS). Figure 4 describes the geometry of an industrial used die. Three geometrical parameters are defined, including the forming angle α , stretching angle β and area reduction ratio η (defined by the initial and final diameters of the CWR sample D_o and D_f), as presented in Fig. 4a. Figure 4b illustrates the simplified die geometry

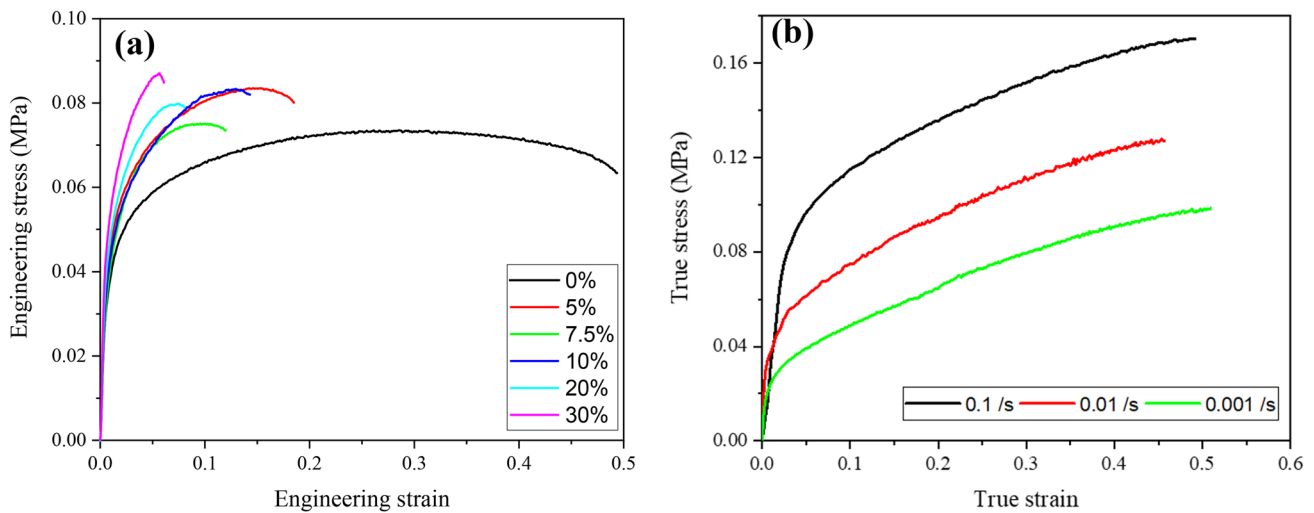


Fig. 2 a Engineering stress–strain curves of plasticine with different flour weight ratios (strain rate 0.5/s); b true strain–stress curves of pure plasticine at different strain rates. (in colour)

for this study, in which a new parameter, the feed angle γ , i.e. the slope of the inclined plate, is defined. These simplified dies enable the stress states in the commercial CWR process to be simulated in a lab environment and forming central cracking.

3.1.3 Experimental procedures

CWR tests were conducted on the plasticine/flour billets to reveal the multiple fracture mechanisms. The flour weight ratio varies from 0 to 30%. Other process parameters were kept consistent such as the die geometry (Reference die in Table 1) and rolling speed (20 mm/s). After the rolling, the sample was sectioned along the axial direction, and the central cracking condition was inspected. If the dimension of the void/crack exceeds 0.5 mm, it is defined as a cracked billet.

CWR tests under various die geometries were conducted for determining the material constants and validating the proposed fracture criterion. Pure plasticine was applied here to simulate the central crack behaviours of high ductility materials such as C45 steel at elevated temperatures. Table 1 describes the dies geometries in five CWR cases.

The Reference die is an industrial used die, referring to the die geometry in literature by Li et al. [11]. Dies in cases 1–4 were simplified ones, based on the Reference case by varying feed angles, aiming to generate various stress states within the workpiece and result in cracked and non-cracked cases for material constants determination.

3.2 Finite element model

The CWR FE model was developed to investigate the stress/strain and damage evolution and validate the proposed fracture criterion, especially for high ductility materials. The model was established in QForm, which is computationally efficient in simulating metal forming processes with large plastic deformation and severe shear effects. Figure 5 illustrates the FE model configuration corresponding to the setup in Fig. 3. The billet is initially located between the two dies. The top and bottom dies move at a relative speed of 20 mm/s. The true stress–strain curves of the pure plasticine in Fig. 2b were employed to describe the visco-plasticity material behaviours, including the hardening and strain rate effects. The data before necking was applied, after which,

Fig. 3 Cross wedge rolling laboratory prototype consisting of an electronically controlled step motor, two 3D printed dies and plasticine workpiece. (in colour)

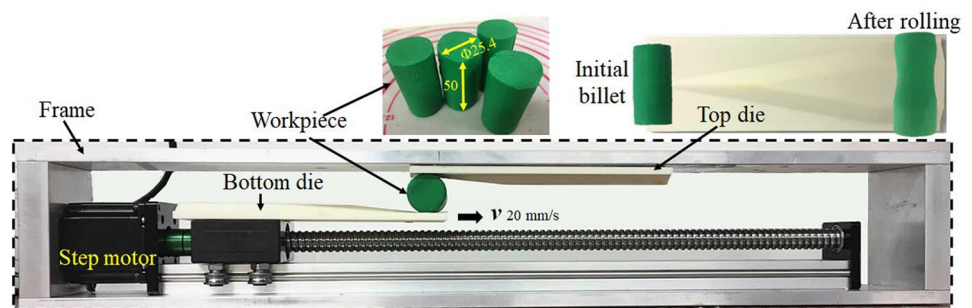
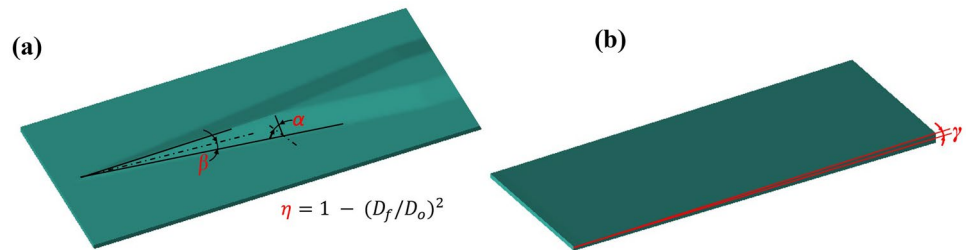


Fig. 4 Die descriptions **a** industrial applied die described by forming angle α , stretching angle β and area reduction ratio η (the initial and final diameters of samples D_o and D_f); **b** simplified dies defined by the feed angle γ . (in colour)



the stress was assumed to keep constant to be the maximum yield stress. The Lévy-Mises equation was applied to describe the material flow, which ignores the elastic deformation due to the strong plastic deformation during the CWR tests as stated in the document [43]. The yield surface was described by the von Mises yield criterion. The density of the pure plasticine was set to be 1868 kg/m^3 by experimental measurement. The Young's modulus was calculated to be 2.6 MPa based on the stress/strain curves, while the Poisson's ratio was set to be 0.4 by averaging the data in the literature [35, 44, 45]. The Coulomb friction model was applied to describe the friction behaviours between the soft plasticine and the rigid dies. The shear stress on the contact interface has never exceeded the shear yield strength because of the automatic shear yield stress correction algorithm in QForm. In the FE simulation, the friction coefficient is less than the limit value of 0.577 , though a friction coefficient of 0.9 was used to avoid slipping between the sample and dies based on careful analyses and comparisons. The damage models were embedded to present the fracture behaviours through the user-defined subroutine programmed by LUA language. Dual mesh strategy was applied to automatically refine the regions in high geometry complexity or intensive stress/strain concentration. The central region (a cylinder with a diameter of 12.5 mm) was further refined with an adapter factor of 1.5 . The total element number of the whole system, for example in case 1, ranges from $196,754$ to $204,742$.

Zhou et al. [24] validated the reliability of the CWR FE model by comparing it with the experiment in terms of the sample final geometry and the inner material flows.

Table 1 Geometric parameters of cross wedge rolling dies

| Case no. | Forming angle $\alpha/^\circ$ | Stretching angle $\beta/^\circ$ | Area reduction ratio $\eta/\%$ | Feed angle $\gamma/^\circ$ |
|-----------|-------------------------------|---------------------------------|--------------------------------|----------------------------|
| Reference | 15 | 7 | 44 | - |
| 1 | 90 | 0 | 44 | 0.91 |
| 2 | 90 | 0 | 61 | 1.37 |
| 3 | 90 | 0 | 75 | 1.83 |
| 4 | 90 | 0 | 94 | 2.74 |

3.3 Damage models and material constants

Ten existing damage models with a high possibility to predict the central cracking accurately are listed in Table 2. The associated material constants for C45 steel in Zhu's model, Smith's model, MMC and X&W model were extracted from the references Zhu and Engelhardt [26] and Bai [30], calculated based on loads of experiments including tensile, shearing tests with flat, round with/without notches. The damage models along with calibrated material constants were embedded into the FE model and compared with the proposed fracture criterion.

The maximum plastic strain criterion is widely applied in predicting ductile fracture due to its simplification. Li and Lovell [22] proved its accuracy when comparing two CWR cases with dies in different shapes. The C&L model, a phenomenological model, has been experimentally validated by various metal forming processes such as extrusion, which emphasises the dominant contribution of the first principal stress to material fracture. Pater [46] applied it to predict the central cracking in hot steels. The stress invariant-related parameter, triaxiality (the ratio of mean stress over the von Mises stress, $\eta_t = \frac{\sigma_m}{\bar{\sigma}}$), is involved in many models such as the classic R&T model, Pater et al. and X&W models, which represents void growth. However, Pater et al. [16] found that the central crack mechanisms in CWR include both void formation and shear fracture. Thus, Pater et al. [16] and Zhou et al. [24] include the shear stress-related parameters, the shear ratio ($\frac{\sigma_1 - \sigma_3}{\bar{\sigma}}$) and the maximum shear stress in the fracture criteria. In order to predict the ductile fracture with shear effects, Zhu and Engelhardt [26] and Smith et al. [25] extended the R&T models by introducing the shear ratio and the void shrinkage, respectively. Nevertheless, the Lode angle parameters such as the normalised Lode angle $\bar{\theta}$ and the normalised third stress invariant ξ are involved in the last two models. The triaxiality-related

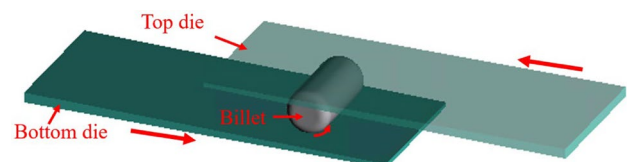


Fig. 5 Configuration of cross wedge rolling finite element model for plasticine. (in colour)

Table 2 Ten existing damage models and the material constants

| Fracture criteria | Equations | Notes |
|---------------------------------------|---|---|
| Maximum plastic strain criterion [22] | $\bar{\epsilon}_f = D_c$ | $\bar{\epsilon}_f$ – Plastic strain to fracture |
| C&L model [46] | $\int_0^{\bar{\epsilon}_f} \sigma^* d\bar{\epsilon}_p = D_c$ | D_c – Critical damage value |
| R&T model [47] | $\int_0^{\bar{\epsilon}_f} \exp(1.5 * \frac{\sigma_m}{\sigma}) d\bar{\epsilon}_p = D_c$ | σ^* – The maximum tensile stress |
| Oyane model [48] | $\int_0^{\bar{\epsilon}_f} (1 + \frac{\sigma_m}{A_0 \sigma}) d\bar{\epsilon}_p = D_c$ | $\bar{\epsilon}_p$ – Equivalent plastic strain |
| Pater et al.'s model [49] | $D_c = \begin{cases} \int_0^{\bar{\epsilon}_f} \left[(1 - f(\eta_t)) \left(\frac{\sqrt{3} \sigma_1 - \sigma_3}{2} \right) + f(\eta_t) \cdot \frac{\sigma_1}{\sigma} \right] d\bar{\epsilon}_p \\ \int_0^{\bar{\epsilon}_f} \frac{\sigma_1}{\sigma} d\bar{\epsilon}_p \end{cases}$ | σ_m – Hydrostatic stress |
| | $f(\eta_t) = 3\eta_t \cdot \sqrt{3\eta_t} \text{ or } (\eta_t)^2$ | $\bar{\sigma}$ – Equivalent von Mises stress |
| | $A\tau_m + B\sigma_1 = D_c; A + B = 1$ | A_0 – Material constant |
| Zhou et al.'s model [24] | $\int_0^{\bar{\epsilon}_f} a_1 \exp(a_2 * \eta_t) (\frac{\sigma_1 - \sigma_3}{\sigma})^{a_3} d\bar{\epsilon}_p = D_c$ | Triaxiality $\eta_t \leq 0$ |
| Zhu and Engelhardt's model [26] | $\int_0^{\bar{\epsilon}_f} b_1 \exp(b_2 * \eta_t) - b_3 \exp(-b_4 * \eta_t) d\bar{\epsilon}_p = D_c$ | $0 < \eta_t \leq 0.333$ |
| Smith et al.'s model [25] | $\int_0^{\bar{\epsilon}_f} \frac{c_1}{c_2} \sqrt{\frac{1+c_2}{3}} \cos(\frac{\pi\theta}{6}) + c_3(\eta_t + \frac{1}{3} \sin(\frac{\pi\theta}{6}))^{-1} d\bar{\epsilon}_p = D_c$ | $\eta_t > 0.333$ |
| MMC model [29] | $\int_0^{\bar{\epsilon}_f} d_1 \exp(-d_2 * \eta_t) - [d_1 \exp(-d_2 * \eta_t) - d_3 \exp(-d_4 * \eta_t)] (1 - \xi^m)^m d\bar{\epsilon}_p = D_c$ | A, B material constants, ranging from -1 to 1 |
| X&W model [50] | | Material constants a_1, a_2, a_3 and $a_4 = 1.37, -2.04, -9.47$ and 1.57 respectively for C45 steel [26] |
| | | Material constants b_1, b_2, b_3 and $b_4 = 2.4, -0.49, 1.5$ and 0.08 respectively for C45 steel [26] |
| | | Normalised lode angle |
| | | $\bar{\theta} = 1 - \frac{2}{\pi} \cos^{-1} \left[\frac{27(\bar{\sigma}_1 - \sigma_m)(\sigma_2 - \sigma_m)(\sigma_3 - \sigma_m)}{2\bar{\sigma}^2} \right]$ |
| | | $c_1 = 753$ MPa, $c_2 = 410$ MPa, $c_3 = 0.137$ and $n = 0.13$ for C45 steel [26, 30] |
| | | The normalised third stress invariant |
| | | $\xi = \frac{2\bar{\sigma}^2}{27(\bar{\sigma}_1 - \sigma_m)(\sigma_2 - \sigma_m)(\sigma_3 - \sigma_m)}$ |
| | | $d_1 = 0.49, d_2 = 0.001, d_3 = 0.76, d_4 = 1.89$, and $m = 6$ for C45 steel [26] |

Table 3 Process parameters of 12 cross wedge rolling tests on C45 steel and the central cracking results

| Ref | Case no | Temperature/°C | Rolling speed/mm/s | Initial billet diameter/mm | Die geometry | | | Cracking condition |
|------|---------|----------------|--------------------|----------------------------|--------------------|-------------------|------------|--------------------|
| | | | | | $\alpha(^{\circ})$ | $\beta(^{\circ})$ | $\eta(\%)$ | |
| | S1 | | | | 15 | 10 | 35.00 | No crack |
| | S2 | | | | 15 | 10 | 55.00 | Cracked |
| | S3 | | | | 15 | 10 | 75.00 | Cracked |
| [13] | S4 | 1100 | 396 | 40 | 15 | 5 | 75.00 | Cracked |
| | S5 | | | | 15 | 7.5 | 75.00 | Cracked |
| | S6 | | | | 20 | 10 | 75.00 | Cracked |
| | S7 | | | | 25 | 10 | 75.00 | No crack |
| | S8 | | | 26 | 15 | 10 | 28.40 | No crack |
| | S9 | 1150 | | 33 | 15 | 10 | 55.60 | Cracked |
| [49] | S10 | | 300 | 40 | 15 | 10 | 69.70 | Cracked |
| | S11 | 1050 | | 33 | 15 | 10 | 55.60 | Cracked |
| | S12 | 1100 | | 33 | 15 | 10 | 55.60 | Cracked |

damage models are applicable to the high triaxialities, while the Lode angle parameters expand its application to the low and negative triaxiality range such as the shear fracture. All these models were examined quantitatively to check its robustness in predicting central cracks in C45 steels.

3.4 Experimental CWR data from literature

3.4.1 High ductility materials: hot C45 steels and pure plasticine

Twelve groups of CWR tests with C45 steels are summarised in Table 3, which was applied to validate the robustness of the investigated damage models. Yang et al. [13] investigated central cracking behaviours by varying different die geometries and keep the temperature and rolling speed constant. Pater et al. [16] investigated the effects of temperature and area reduction ratio on central cracking under the same rolling speed and the same forming and stretching angles. The temperature and rolling speed in all the listed cases vary in a narrow range. Their effects in the fracture have been included in the constitutive model by affecting the stress/strain distributions. Thus, the temperature and the strain rate are not considered in the newly proposed fracture criterion. The cracking results of Pater's research of cases S8–S10 are consistent with Yang's results in cases S1–S3, i.e. the increase of area reduction ratio accelerates the central cracking formation.

3.4.2 Low ductility materials: pure aluminium and plasticine/flour composite

The robustness of the previously proposed fracture criterion for low ductility materials has been validated by 27 groups of pure aluminium AA1100 H16 CWR cases and the 16 groups of plasticine/flour composite CWR cases.

The experimental data for pure aluminium can be found in Table 1 in Zhou et al. [24] and Tables 3 and 4 in Zhou et al. [17]. These data were revisited to validate the high robustness of the proposed fracture criterion in different materials.

4 Experimental and finite element results

4.1 Multiple central crack mechanisms

4.1.1 In plasticine/flour composites with various ductility

Figure 6 indicates that the material ductility varies with the plasticine–flour weight ratio. The fracture strain was obtained by conducting uniaxial tensile tests, as shown in

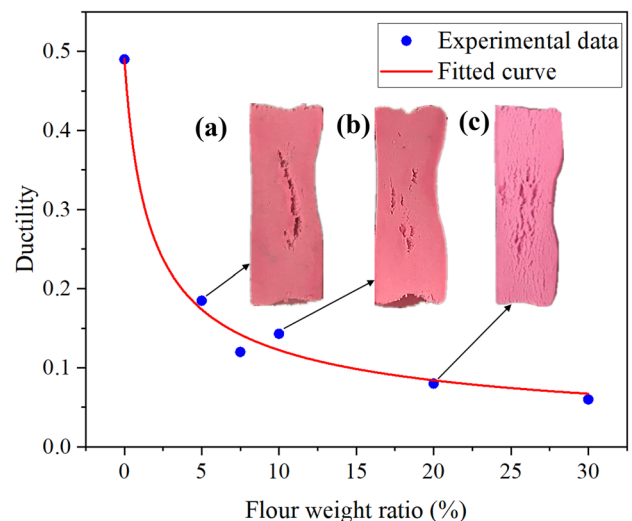


Fig. 6 The variety of material ductility over the plasticine and flour weight ratios, along with the longitudinal sections of three selected rolled samples in (a), (b), and (c). (in colour)

Fig. 7 Comparison of fracture morphologies of cross wedge rolled samples on **a** pure aluminium [11] and **b** C45 steel [16]. (in colour)

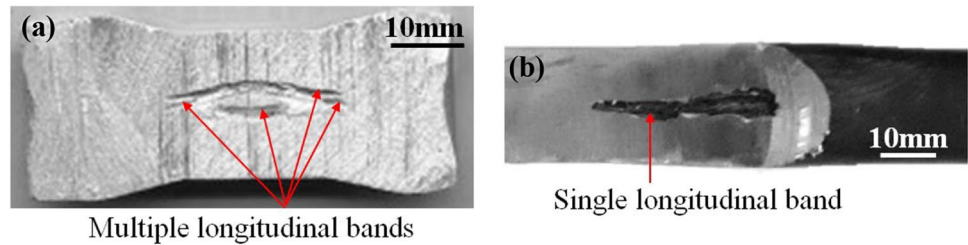
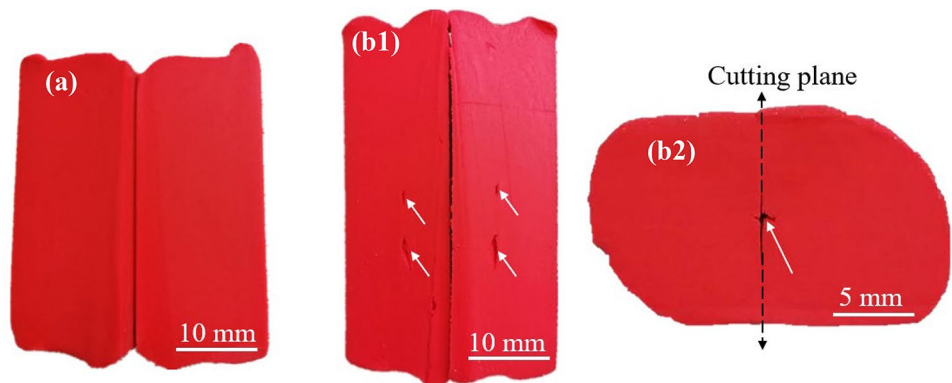


Fig. 2a. The strain at the fracture points was defined as the fracture strain. The longitudinal sections of the rolled samples made by the corresponding materials are presented. The general trend is that the ductility reduces as the flour weight ratio increases. The sectioned samples demonstrate the transition of the central crack mechanism. At the flour ratio of 5%, only one dominant axial crack appears within the material, as shown in Fig. 6a. Then, with the increase of the flour content, more cracks appear (in Fig. 6b). In the end, when the flour ratio reaches 20%, many minor cracks scatter on the whole surface (in Fig. 6c). It is reasonable to attribute it to different ductility. In Fig. 6a, the material is ductile ($\epsilon_f=18.5\%$) and capable to bear high plastic deformation before final fracture; thus, the fracture only occurs in the central region but not on the subsurface or at the sample ends. In Fig. 6c, when the material is brittle ($\epsilon_f=8\%$) with limited capacity for plastic deformation, minor cracks scatter across the whole cross section, consistent with the feature of brittle fracture.

4.1.2 In pure aluminium and hot steels

The multiple fracture mechanisms found in plasticine/flour composites, that is transferring from brittle to ductile fracture with the ductility increase, also apply to metals. As shown in Fig. 7a, multiple axial cracking bands were observed in the pure aluminium AA1100 H16 during CWR, which was attributed to the low ductility (~8%) [51], while the limited axial longitudinal cracks were found in the investigations of Yang et al. [13] and Pater et al. [52] on the C45 steels due to the ductile fracture nature (~39%) [53] as seen in Fig. 7b.

Fig. 8 Crack conditions in the rolled samples after cross wedge rolling: **a** crack-free (case 2 in Table 1) and **b** cracked (case 3 in Table 1) on **b1** longitudinal section and **b2** transverse section (the central cracks are indicated by the white arrows and the dashed black arrows show the cutting plane). (in colour)



4.2 Central cracking criterion

4.2.1 Results of cross wedge rolling test on pure plasticine under various die geometries

The cracking conditions of plasticine samples after rolling in Table 1 in this study were used to examine the damage models. Figure 8 presents the crack-free and cracked rolled samples. In Fig. 8a, no voids/cracks were noticed on the sectioned surfaces, while in Fig. 8b, evident central cracks were observed on both the longitudinal and the transverse view. The cracks, located in the central region along the axial direction, is consistent with the central cracks observed in hot steels by Pater et al. [16]. For all the cases in Table 1, central cracking only occurred in case 3 because of the high ductility of pure plasticine and narrow forming window for central cracking.

4.2.2 Validation of the proposed fracture criterion by plasticine with various ductility

Figure 9 compares the normalised damage value ($D_n = D/D_c$) on two plasticine materials in 21 CWR cases to validate the robustness of the proposed central crack in various materials. The first 16 cases for low ductility were obtained from Tables 3 and 4 in the study of Zhou et al. [17], represented by green symbols and labelled as P1–P16 in Fig. 9. The ductility of the applied plasticine/flour composite was 12%. The proposed fracture criterion for low ductility materials was applied for the damage prediction.

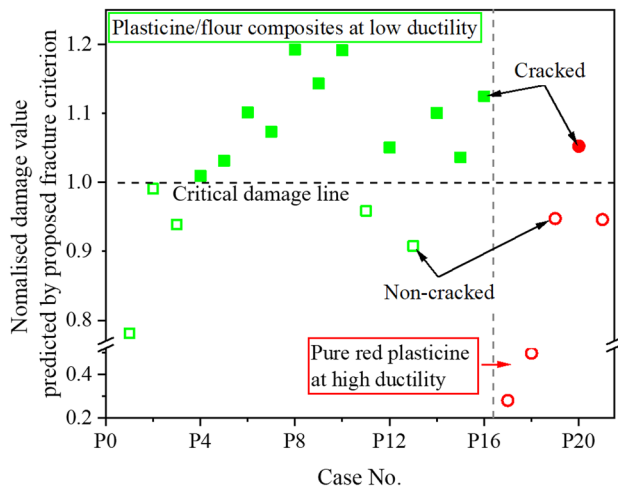


Fig. 9 Normalised damage value on plasticine with different ductile levels predicted by the proposed fracture criterion (the hollowed symbols present the crack-free cases, while the solid cases present the cracked cases; the green cases present the cases conducted with low ductility material, with the red ones for high ductility materials). (in colour)

The last five cases P17–P21 correspond to the Ref case and cases 1–4 in Table 1. The proposed fracture criterion for high ductility was applied due to the high ductility of the pure plasticine, ~50%. Cases 2–4 were conducted to determine the associated material constants, with the rest two cases for the validation. The value *C* and the critical

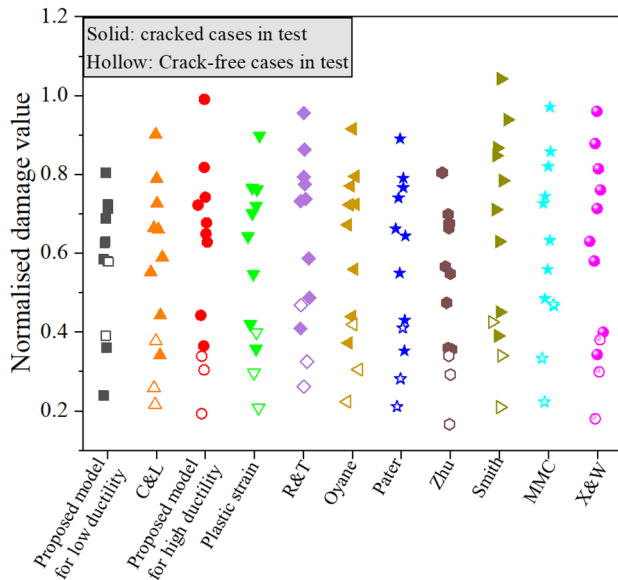


Fig. 10 Normalised damage values of the central point at the end of 12 C45 CWR cases predicted by 11 damage models (each column contains 3 hollow symbols and 9 solid symbols, representing 3 crack-free cases and 9 cracked cases observed in experiments). (in colour)

damage value were calculated to be 1 and 1.07 MPa, respectively. The predicted damage values in the Ref case and case 1 were calculated to be lower than the critical value 1.07 MPa, which matched the experimental observations that no cracking occurred in these two cases. Note that the cut-off value of triaxiality at -0.33 is applied. Bao [54] and Bao and Wierzbicki [55] experimentally verified that fracture would not happen in ductile materials when the triaxiality is less than -0.33 .

The normalised damage values in all the cracked cases are scattered above the critical line $y = 1$, while the values of all the non-cracked cases are all below the critical line, implying the high accuracy of the proposed fracture criterion in predicting central cracks for both high and low ductility materials.

4.2.3 Examination of 11 damage models by hot C45 steels

Comparison of the 11 damage models Figure 10 summarises the damage values at the sample central point in 12 CWR cases predicted by 11 damage models. The 12 CWR experimental cases refer to the 12 C45 steel cases listed in Table 3, and the 11 damage models include the 10 listed in Table 2 and the newly proposed one in Eq. (2). In Fig. 10, the horizontal axle represents the 11 damage models, and the vertical axle presents the normalised damage value, calculated by dividing the damage value acquired from the FE model by a constant. This constant varies according to different models, enabling the normalised value ranging from 0 to 1. The material constants associated with the damage models were mainly extracted from the references, as listed in Table 2, while for the proposed model, they were obtained by simulating all 12 groups of C45 CWR test in Table 3 and calibrating against the experimental cracking results. The calculated value for the material constant *C* is zero in this case. The normalised damage values from 11 damage models are presented in 11 columns. There are 12 symbols in each column, 9 solid and 3 hollow ones, corresponding to the 9 cracked cases and 3 non-cracked cases in Table 3. It is expected that with a robust fracture criterion, the predicted damage value in all the cracked cases is higher than the damage value in the non-cracked cases. In Fig. 10, only the proposed model for high ductility and the Zhu’s model are capable of distinguishing the solid symbols from the hollow ones, which means that all the solid symbols are above all the hollow ones. This implies the high accuracy of these two models in predicting central cracking in C45 steels.

For all the other models, the solid and hollow symbols are mixed together. The same pattern is noticed in the rest of the models (except for the proposed model for low ductility) that the two hollow symbols are at the lowest of each column, followed by a solid one above them and then the

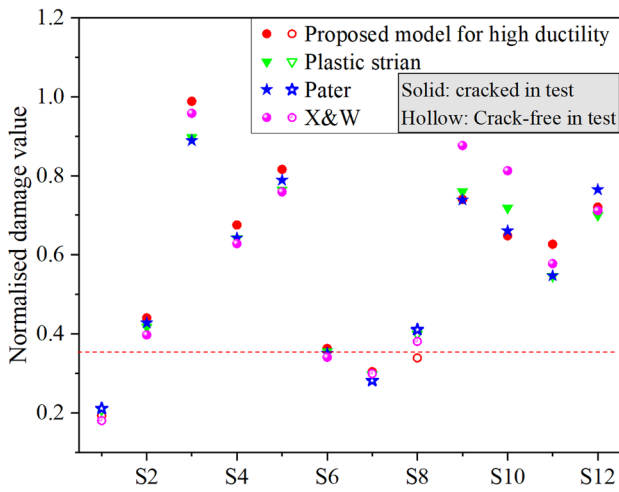


Fig. 11 Damage value distribution of the central point at the end of CWR cases listed in Table 2 predicted by four damage models. (in colour)

third hollow one, leaving all the other solid symbols above. Four damage models, namely, the proposed model for high ductility, Pater’s model, the maximum plastic strain criterion and X&W model, are taken as examples for a closer examination, as shown in Fig. 11, where the horizontal axis presents the 12 C45 steel cases listed in Table 3. For all the four damage models, the highest damage value for the non-cracked cases was predicted to occur in case S8 and the lowest value for the cracked cases was predicted in case S6. Only in the proposed damage model, the damage value in case S6 was higher than that in case S8, agreeing with the experiment that central crack occurred in case S6 but not S8. Another similar trend was noticed in the four models, that is the damage value increases or decreases with the variation of the plastic strain among these 12 cases. It implies

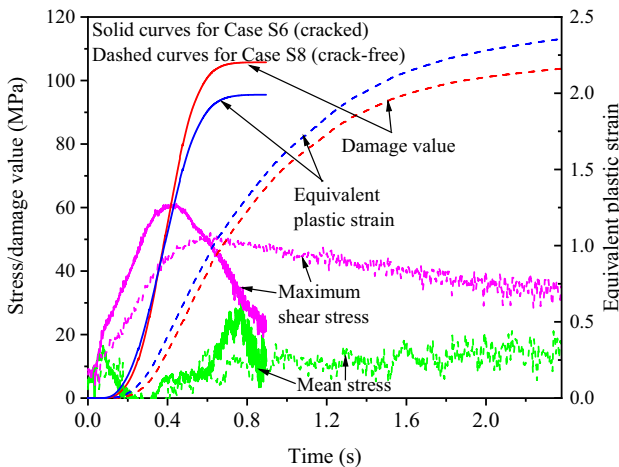


Fig. 12 Comparison of cracked and non-cracked cases in stress/strain and damage evolution. (in colour)

the significance of plastic strain in predicting central crack formation. The slight difference between the trends under the damage models indicated the importance of stress state on the damage evolution.

Damage analysis under the proposed fracture criterion Figure 12 compares the stress/strain and damage evolution in case S6 (cracked) and S8 (crack-free), which clearly demonstrates how the stress state influences the cracking behaviours in high ductility material. In both cases, the stress variables (the maximum shear stress and the mean stress) increased at the early stage at around 0.5 s, but the stress values in case S6 increased quickly and reached a much higher value. Similarly, the plastic strain increased quickly in a short time. Although the final equivalent plastic strain in case S6 is less than that in case S8, it does not affect the higher accumulated damage value in case S6.

Thus, the equivalent plastic strain can generally control the damage variation trend, but to get accurate predictive results in complex situation such as in CWR, the stress variables must be considered.

5 Discussion

5.1 Multiple central crack mechanisms

The multiple central crack modes under different material ductility are observed in Figs. 6 and 7. Figure 13 systematically illustrates the central crack formation and evolution. During CWR, the workpiece is self-rotated under the dies (in Fig. 13a). There are defects such as inclusion and microvoids within the material (in Fig. 13b). Under slight deformation (in Fig. 13c), the microvoids are rotated and elongated slightly, and voids form between the inclusion and material matrix. For the low ductility materials such as pure aluminium (highly strained), with the increase of the maximum shear stress and the first principal stress, multiple sharp edges form around the voids (with/without inclusions), which are subjected to the high-stress concentration caused by the limited plastic deformation (in Fig. 13d1). The maximum shear stress sharpens the crack ends, while the first principal stress accelerates the crack opening. Both of these stresses are associated with workpiece rotation, which in turn accelerates the crack propagation along with multiple directions (in Fig. 13e2). This causes multiple cracking bands to be observed, as shown in Figs. 6c and 7a.

Nevertheless, in high ductility materials such as hot C45 steels, the stress concentration is weakened due to their capability of bearing severe plastic deformation.

Instead of sharp cracking points, micro-voids form (in Fig. 13d2). As the sample rotates further, the maximum shear stress increases gradually. This increased stress causes the voids and the adjacent materials to be distorted and elongated. As a result, intense stresses concentrate at the void ends to accelerate the void coalescences and facilitate the formation of new voids. The mean stress accelerates the void growth, facilitating the void coalescences. With their combined effects, the voids grow, coalesce and finally link to macrocracks (in Fig. 13e2). Thereby, two main fracture modes take place, i.e. shear fracture and void formation, corresponding to two main fracture mechanisms, void distortion and void growth. The central cracking mechanisms keep consistent with the investigations made by Pater et al. [16], Yang et al. [13] and Zhou et al. [19].

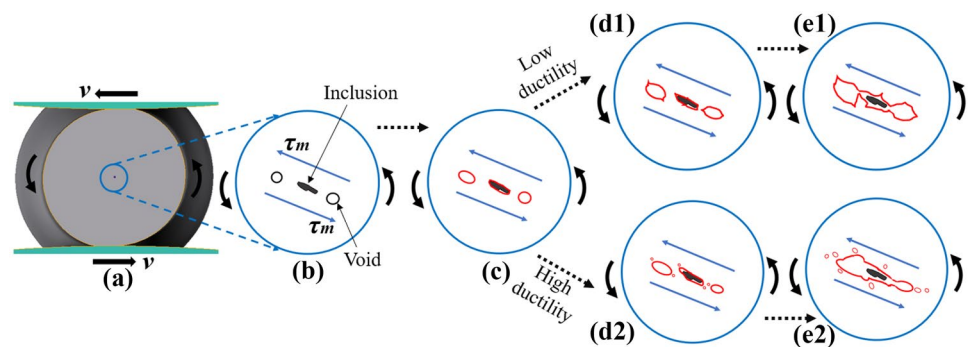
5.2 Central crack damage model set

The significance of plastic strain and stress states in ductile fracture has been acknowledged and considered in many damage models. Wierzbicki et al. [50] state that the C&L model emphasises the dominant effect of the first principal stress, while its applicability was experimentally proved in low or negative triaxiality. In CWR, the triaxiality varies in a wide range. Both the R&T model and the Oyane model described the void growth. Later on, Smith et al. [25] expanded the application of the R&T model from high triaxiality to low triaxiality by introducing void shrinkage. However, none of them considers shear effects, which are generally considered the driving force in CWR. The introduced Lode angle parameters enable ductile fracture prediction in low or negative triaxialities, such as shear fracture. However, the MMC model developed by Bai and Wierzbicki [29] was applicable in monotonic loading conditions, while cyclic loadings are involved in CWR. Wierzbicki et al.

[50] developed the X&W fracture criterion showing high accuracy in a wide range of stress states considering triaxiality and Lode parameter, but similarly, its application is limited in the monotonic loading conditions. Pater's model considers both the void formation and shear fracture in a hybrid damage model. The involved C&L model was applied for the high triaxiality; however, Wierzbicki et al. [50] proved this model worked well only in low or negative triaxialities. Zhu's model adapted the R&T model with the consideration of shear effects, the prediction of which agrees well with the experimental observation in the 12 CWR cases, as shown in Fig. 10. However, four independent material constants are included in Zhu's model, which could be practically nontrivial to be determined, especially at elevated temperatures. Similarly, some non-linear damage models have recently been developed to predict the ductile fracture under non-proportional loading conditions, such as the one proposed by Bai [30] and further validated by Papisidero et al. [33]; however, many material constants are associated, which cannot be easily achieved, especially at elevated temperatures. Thus, they are unsuitable for industrial applications. Regarding the new fracture criterion proposed in this study, only one pair of simple dies and three CWR tests is required to determine the one material constant. The simplification of this model and the extremely simple calibration process for the material constants will bring considerable benefits to industrial applications.

However, the ductile central crack damage model is only workable for high ductility materials. Its incapability of predicting the central cracking in low ductility materials, the green flour/plasticine composite (ductility 12%) and the pure aluminium AA1100 H16 (ductility around 8%), is demonstrated in Fig. 14. Neither groups of cracked nor non-cracked cases could be distinguished by a critical value in both cases due to the different fracture natures in materials with various ductility.

Fig. 13 Schematics of multiple central crack mechanisms: **a** minimum cross-section of workpiece during cross wedge roiling; **b** initial state in the central region including voids and inclusion; **c** state with slight deformation; crack nucleation and propagation for **d1**, **e1** low ductility and **d2**, **e2** high ductility. (in colour)



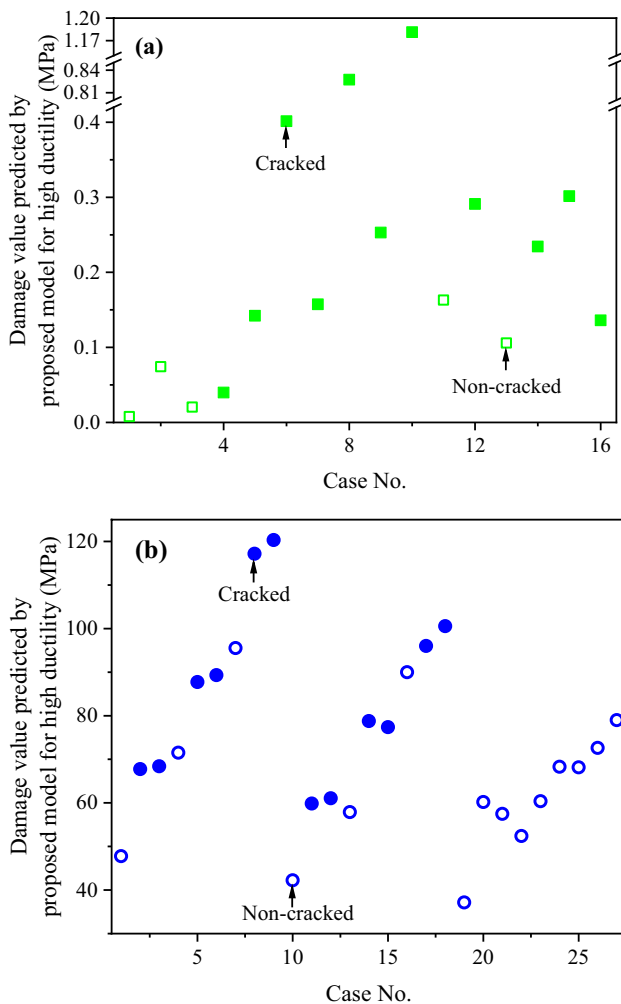


Fig. 14 Damage value on the low ductility material predicted by the damage model for high ductility **a** green plasticine with flour; **b** Pure Al AA1100 H16. (in colour)

6 Conclusions

In this research, the central cracking mechanisms over different materials with varying ductility were revealed experimentally. A physics-based central cracking prediction model was proposed and validated by 60 groups of CWR tests and by comparing with the other ten damage model. A lab-scale CWR prototype was made to reproduce the stress–strain conditions during the commercial CWR process. The corresponding FE model was developed to track the stress/strain/damage evolutions. New plasticine/flour composites were designed to reveal the materials ductility effects on central crack mechanisms. The following conclusions can be drawn:

1. A physics-based damage model set was proposed for predicting the central crack formation. The robustness of this damage model set was validated by 60 groups of

CWR experimental data under different stress states and with various materials including hot steels, pure aluminium and plasticine/flour composites. Its high accuracy was also proved by comparing with other ten existing damage models/fracture criteria. This unified damage model set can effectively drive the development of CWR by producing products without any internal defects.

2. The central cracking mechanism for high ductility materials was investigated in particular. The equivalent plastic strain and the maximum shear stress play dominant roles in forming central cracking in high ductility materials. The equivalent plastic strain facilitates forming voids instead of sharp cracks. The maximum shear stress associated with the mean stress accelerates the void distortion and growth, driving void coalescence and propagation. Their joint effects cause the final macroscopic central crack formation.
3. The multiple central crack mechanisms were revealed in different materials with different ductility. In low ductility materials, crack-driven fracture dominates, while in high ductility materials, the fracture is driven by voids. The central cracking in low ductility materials was accurately predicted by the stress-based fracture criterion, while the energy-based damage model shows high prediction accuracy in high ductility materials such as hot steels and pure plasticine.

Author contribution Xianyan Zhou: conceptualization, methodology, software, investigation, validation, formal analysis, writing—original draft preparation. Chaoyang Sun: writing—review and editing, visualisation, funding acquisition. Baoyu Wang: writing—review and editing, investigation, resources. Jun Jiang: supervision, conceptualization, methodology, writing—review and editing, funding acquisition.

Funding Great appreciation is given to the Beijing Institute of Aeronautical Materials (BIAM) for the financial support. The research was performed at the BIAM-Imperial Centre for Materials Characterisation, Processing and Modelling at Imperial College London. The authors also gratitude the financial support from the Royal Society-Newton Mobility Grant (IECNSFC181520). Xianyan Zhou acknowledges the Chinese Scholarship Council (Grant Number: 201606950020) for her bursary.

Availability of data and material The data that support the findings of this study are openly available, such as in <https://doi.org/10.1016/j.jmatprotec.2017.09.041> and <https://doi.org/10.1016/j.ijmecsci.2019.105274>.

Code availability Not applicable.

Declarations

Ethics approval Not applicable.

Consent to participate Not applicable.

Consent for publication The authors consented to publish this article.

Conflict of interest The authors declare no competing interests.

Open Access This article is licensed under a Creative Commons Attribution 4.0 International License, which permits use, sharing, adaptation, distribution and reproduction in any medium or format, as long as you give appropriate credit to the original author(s) and the source, provide a link to the Creative Commons licence, and indicate if changes were made. The images or other third party material in this article are included in the article's Creative Commons licence, unless indicated otherwise in a credit line to the material. If material is not included in the article's Creative Commons licence and your intended use is not permitted by statutory regulation or exceeds the permitted use, you will need to obtain permission directly from the copyright holder. To view a copy of this licence, visit <http://creativecommons.org/licenses/by/4.0/>.

References

- Fu XP, Dean TA (1993) Past developments, current applications and trends in the cross wedge rolling process. *Int J Mach Tools Manuf* 33:367–400. [https://doi.org/10.1016/0890-6955\(93\)90047-X](https://doi.org/10.1016/0890-6955(93)90047-X)
- Shu X, Shi J, Chen J, Yang H (2021) Effects of process parameters on surface quality of shaft parts formed by warm cross-wedge rolling. *Int J Adv Manuf Technol*. <https://doi.org/10.1007/s00170-021-06784-2>
- Shchukin VY, Kozhevnikova GV, Petrenko VV (2012) Cross-wedge rolling at pti nas Belarus. *Appl Mech Mater* 198–1202
- Ji H, Liu J, Fu X et al (2017) Finite element analysis and experiment on multi-wedge cross wedge rolling for asymmetric stepped shaft of C45. *J Cent South Univ* 24:854–860. <https://doi.org/10.1007/s11771-017-3487-8>
- Zheng Z, Wang B, Hu Z (2012) Study on roller profile for cam forming by cross wedge rolling. *Appl Mechan Mater*
- Pater Z, Gontarz A, Tofil A (2011) Analysis of the cross-wedge rolling process of toothed shafts made from 2618 aluminium alloy. *J Shanghai Jiaotong Univ*. <https://doi.org/10.1007/s12204-011-1119-2>
- Bulzak T, Pater Z, Tomczak J, Majerski K (2020) Hot and warm cross-wedge rolling of ball pins - comparative analysis. *J Manuf Process*. <https://doi.org/10.1016/j.jmapro.2019.12.001>
- Shi J, Liu J, Wang B, Shen J (2022) Numerical and experimental research on warm cross wedge rolling of hollow shafts with corrugated surface. *Int J Adv Manuf Technol* 2022:1–20. <https://doi.org/10.1007/S00170-022-09379-7>
- Wu ZJ, Peng WF, Shu XD (2017) Influence of rolling temperature on interface properties of the cross wedge rolling of 42CrMo/Q235 laminated shaft. *Int J Adv Manuf Technol* 91:517–526. <https://doi.org/10.1007/s00170-016-9734-6>
- Peng WF, Zhang JH, Huang GX et al (2016) Stress distributions during the cross-wedge rolling of composite 42CrMo/Q235 laminated shafts. *Int J Adv Manuf Technol* 83:145–155. <https://doi.org/10.1007/s00170-015-7541-0>
- Li Q, Lovell MR, Slaughter W, Tagavi K (2002) Investigation of the morphology of internal defects in cross wedge rolling. *J Mater Process Technol* 125–126:248–257. [https://doi.org/10.1016/S0924-0136\(02\)00303-5](https://doi.org/10.1016/S0924-0136(02)00303-5)
- Li Q, Lovell M (2008) Cross wedge rolling failure mechanisms and industrial application. *Int J Adv Manuf Technol* 37:265–278. <https://doi.org/10.1007/s00170-007-0979-y>
- Yang C, Dong H, Hu Z (2018) Micro-mechanism of central damage formation during cross wedge rolling. *J Mater Process Technol* 252:322–332. <https://doi.org/10.1016/j.jmatprotec.2017.09.041>
- Zhou J, Yu Y, Zeng Q (2014) Analysis and experimental studies of internal voids in multi-wedge cross wedge rolling stepped shaft. *Int J Adv Manuf Technol* 72:1559–1566. <https://doi.org/10.1007/s00170-014-5768-9>
- Pater Z, Tomczak J, Bulzak T et al (2021) Prediction of ductile fracture in skew rolling processes. *Int J Mach Tools Manuf*. <https://doi.org/10.1016/j.ijmactools.2021.103706>
- Pater Z, Tomczak J, Bulzak T et al (2020) Assessment of ductile fracture criteria with respect to their application in the modeling of cross wedge rolling. *J Mater Process Technol*. <https://doi.org/10.1016/j.jmatprotec.2019.116501>
- Zhou X, Shao Z, Zhang C et al (2020) The study of central cracking mechanism and criterion in cross wedge rolling. *Int J Mach Tools Manuf*. <https://doi.org/10.1016/j.ijmactools.2020.103647>
- Anderson TL (2012) *Fracture mechanics: fundamentals and applications*
- Zhou X, Shao Z, Tian F et al (2020) Microstructural effects on central crack formation in hot cross-wedge-rolled high-strength steel parts. *J Mater Sci* 55:9608–9622. <https://doi.org/10.1007/s10853-020-04677-5>
- Zhang SH, Deng L, Che LZ (2022) An integrated model of rolling force for extra-thick plate by combining theoretical model and neural network model. *J Manuf Process*. <https://doi.org/10.1016/j.jmapro.2021.12.063>
- Zhang SH, Deng L, Tian WH et al (2022) Deduction of a quadratic velocity field and its application to rolling force of extra-thick plate. *Comput Math with Appl*. <https://doi.org/10.1016/j.camwa.2022.01.024>
- Li Q, Lovell MR (2004) The establishment of a failure criterion in cross wedge rolling. *Int J Adv Manuf Technol* 24:180–189. <https://doi.org/10.1007/s00170-003-1607-0>
- Jia Z, Ji J, Wang Y, Wei B (2020) Influence of die parameters on internal voids during multi-wedge-multi-pass cross-wedge rolling. *Int J Adv Manuf Technol*. <https://doi.org/10.1007/s00170-020-05897-4>
- Zhou X, Shao Z, Pruncu CI et al (2020) A study on central crack formation in cross wedge rolling. *J Mater Process Technol*. <https://doi.org/10.1016/j.jmatprotec.2019.116549>
- Smith C, Kanvinde A, Deierlein G (2017) A local criterion for ductile fracture under low-triaxiality axisymmetric stress states. *Eng Fract Mech* 169:321–335. <https://doi.org/10.1016/j.engfracmech.2016.10.011>
- Zhu Y, Engelhardt MD (2018) Prediction of ductile fracture for metal alloys using a shear modified void growth model. *Eng Fract Mech* 190:491–513. <https://doi.org/10.1016/j.engfracmech.2017.12.042>
- Bao Y, Wierzbicki T (2004) On fracture locus in the equivalent strain and stress triaxiality space. *Int J Mech Sci* 46:81–98. <https://doi.org/10.1016/j.ijmecsci.2004.02.006>
- Wierzbicki T, Xue L (2005) On the effect of the third invariant of the stress deviator on ductile fracture. Cambridge
- Bai Y, Wierzbicki T (2010) Application of extended Mohr-Coulomb criterion to ductile fracture. *Int J Fract* 161:1–20. <https://doi.org/10.1007/s10704-009-9422-8>
- Bai Y (2008) Effect of loading history on necking and fracture. *Technology* 1–262
- Benzerger AA, Surovik D, Keralavarma SM (2012) On the path-dependence of the fracture locus in ductile materials - analysis. *Int J Plast*. <https://doi.org/10.1016/j.ijplas.2012.05.003>
- Faleskog J, Barsoum I (2013) Tension-torsion fracture experiments - part I: experiments and a procedure to evaluate the equivalent

- plastic strain. *Int J Solids Struct* 50:4241–4257. <https://doi.org/10.1016/j.ijsolstr.2013.08.029>
33. Papisidero J, Doquet V, Mohr D (2015) Ductile fracture of aluminum 2024–T351 under proportional and non-proportional multi-axial loading: Bao-Wierzbicki results revisited. *Int J Solids Struct* 69–70:459–474. <https://doi.org/10.1016/j.ijsolstr.2015.05.006>
 34. Chijiwa K, Hatamura Y, Hasegawa N (1981) Characteristics of plasticine used in the simulation of slab in rolling and continuous casting. *Trans Iron Steel Inst Jpn*. <https://doi.org/10.2355/isijinternational1966.21.178>
 35. Wong SF, Hodgson PD, Chong CJ, Thomson PF (1996) Physical modelling with application to metal working, especially to hot rolling. *J Mater Process Technol* 62:260–274. [https://doi.org/10.1016/0924-0136\(95\)02219-8](https://doi.org/10.1016/0924-0136(95)02219-8)
 36. Wójcik L, Pater Z, Bulzak T, Tomczak J (2020) Physical modeling of cross wedge rolling limitations. *Materials (Basel)*. <https://doi.org/10.3390/ma13040867>
 37. Zhou W, Lin J, Dean TA, Wang L (2018) Analysis and modeling of a novel process for extruding curved metal alloy profiles. *Int J Mech Sci*. <https://doi.org/10.1016/j.ijmecsci.2018.02.028>
 38. Zhou W, Yu J, Lin J, Dean TA (2020) Effects of die land length and geometry on curvature and effective strain of profiles produced by a novel sideways extrusion process. *J Mater Process Technol*. <https://doi.org/10.1016/j.jmatprotec.2020.116682>
 39. Danno A, Tanaka T (1984) Hot forming of stepped steel shafts by wedge rolling with three rolls. *J Mech Work Technol* 9:21–35. [https://doi.org/10.1016/0378-3804\(84\)90091-3](https://doi.org/10.1016/0378-3804(84)90091-3)
 40. Fu X, Dean T (1991) A study of defects in cross wedge rolling. *Tech Rep* 4
 41. Pater Z, Walczuk P, Lis K, Wójcik Ł (2018) Preliminary analysis of a rotary compression test. *Adv Sci Technol Res J* 12:77–82. <https://doi.org/10.12913/22998624/86812>
 42. Hawryluk M, Polak S, Gronostajski Z, Jaśkiewicz K (2019) Application of physical similarity utilizing soft modeling materials and numerical simulations to analyse the plastic flow of UC1 steel and the evolution of forces in a specific multi-operational industrial precision forging process with a constant-velocity. *Exp Tech* 43:225–235. <https://doi.org/10.1007/s40799-018-0288-4>
 43. Micas Simulations Limited (2017) Theoretical basis of QForm. <https://www.qform3d.com/>
 44. Mott PH, Roland CM (2009) Limits to Poisson's ratio in isotropic materials. *Phys Rev B - Condens Matter Mater Phys*. <https://doi.org/10.1103/PhysRevB.80.132104>
 45. Buchely MF, Maranon A, Silberschmidt VV (2016) Material model for modeling clay at high strain rates. *Int J Impact Eng* 90:1–11. <https://doi.org/10.1016/j.ijimpeng.2015.11.005>
 46. Pater Z (2014) Cross-wedge rolling. Elsevier
 47. Rice JR, Tracey DM (1969) On the ductile enlargement of voids in triaxial stress fields*. *J Mech Phys Solids* 17:201–217. [https://doi.org/10.1016/0022-5096\(69\)90033-7](https://doi.org/10.1016/0022-5096(69)90033-7)
 48. Novella MF, Ghiotti A, Bruschi S, Bariani PF (2015) Ductile damage modeling at elevated temperature applied to the cross wedge rolling of AA6082-T6 bars. *J Mater Process Technol* 222:259–267. <https://doi.org/10.1016/j.jmatprotec.2015.01.030>
 49. Pater Z, Tomczak J, Bulzak T (2020) Establishment of a new hybrid fracture criterion for cross wedge rolling. *Int J Mech Sci* 167:105274. <https://doi.org/10.1016/j.ijmecsci.2019.105274>
 50. Wierzbicki T, Bao Y, Lee YW, Bai Y (2005) Calibration and evaluation of seven fracture models. *Int J Mech Sci* 47:719–743. <https://doi.org/10.1016/j.ijmecsci.2005.03.003>
 51. Li Q (2003) Characterization of failure mechanisms in cross wedge rolling. University of Pittsburgh
 52. Pater Z, Tomczak J, Bulzak T (2020) Rapid estimation of ductile crack formation in cross-wedge rolling. *J Mater Res Technol* 9:14360–14371. <https://doi.org/10.1016/j.jmrt.2020.10.046>
 53. Tao X (2011) Research of damage and fracture for cross wedge rolling based on damage mechanics. China Academy of Machinery Science and Technology Group Co., Ltd
 54. Bao Y (2003) Prediction of ductile crack formation in uncracked bodies
 55. Bao Y, Wierzbicki T (2005) On the cut-off value of negative tri-axiality for fracture. *Eng Fract Mech* 72:1049–1069. <https://doi.org/10.1016/j.engfracmech.2004.07.011>

Publisher's Note Springer Nature remains neutral with regard to jurisdictional claims in published maps and institutional affiliations.